DIRECT NUMERICAL SIMULATION OF FORCED AIR CONVECTION IN ROUGH CHANNELS WITH VARIABLE PHYSICAL PROPERTIES

Alessandro Ceci
Gran Sasso Science Institute
Viale F. Crispi, 7, 67100, L'Aquila, Italy
alessandro.ceci@gssi.it

Davide Modesti
Gran Sasso Science Institute
Viale F. Crispi, 7, 67100, L'Aquila, Italy
davide.modesti@gssi.it

ABSTRACT

We perform direct numerical simulations of turbulent channel flow over Gaussian roughness using air as working fluid, accounting for temperature-dependent viscosity and thermal conductivity. Rough-wall cases are compared with corresponding smooth-wall configurations at matched mean-to-wall temperature ratio, allowing the isolated assessment of variable-property effects on momentum and heat transfer.

The velocity and thermal roughness functions, ΔU^+ and $\Delta\Theta^+$, are evaluated including a virtual-origin correction to maximize the logarithmic-region plateau. The velocity roughness function exhibits a robust behavior across all conditions: when expressed in viscous units, the results show good agreement with incompressible Nikuradse's data, both for the untransformed velocity shift and the one calculated using compressibility transformations. Variable-property effects primarily modulate the magnitude of ΔU^+ through changes in viscous scaling, while the dependence of ΔU^+ on the viscous-scaled roughness height k_s^+ remains consistent with the incompressible trend.

In contrast, the thermal roughness function displays a markedly more complex response. Cooling reduces $\Delta\Theta^+$, whereas heating produces a moderate increase at low Reynolds number but a weaker and non-monotonic effect at higher Reynolds numbers. As a result, no clear universal scaling analogous to the velocity case is observed.

The friction coefficient follows a consistent ordering with the temperature ratio, reflecting the trends in ΔU^+, while the Stanton number exhibits a more scattered behavior due to the competing effects of turbulent transport and molecular diffusion under variable-property conditions.

These results indicate that, while momentum transfer over rough walls retains a quasi-universal character, heat transfer is significantly more sensitive to variable-property effects, motivating the development of transformation frameworks for predictive modeling.

INTRODUCTION

The prediction of heat and momentum transfer in wall-bounded turbulence is central to a wide range of engineering applications, including turbine blade cooling, nuclear reactors, and additive manufacturing, where surfaces are rarely hydraulically smooth and departures from constant-property conditions are often significant. Surface roughness enhances momentum and scalar transport through increased turbulence production and form drag, while variations of thermophysical properties modify both viscous and diffusive processes, altering the near-wall structure of the flow. Classical correlations such as those of Dittus & Boelter (1933); Gnielinski (1976) were derived for smooth-wall flows with constant properties and are known to provide reliable predictions only within limited operating conditions. Empirical corrections, e.g. the Sieder–Tate relation (Sieder & Tate, 1936), attempt to incorporate viscosity variations through bulk-to-wall property ratios, but remain fluid-dependent and often lack predictive capability when large temperature gradients or complex geometrical features are present.

Direct numerical simulation (DNS) has significantly advanced the understanding of wall-bounded turbulence, documenting the role of surface roughness in breaking the universality of inner scaling and modifying the logarithmic layer structure (Jiménez, 2004; Chung *et al.*, 2021). At the same time, DNS studies of variable-property flows have shown that density, viscosity and thermal diffusivity variations can strongly affect turbulence statistics, near-wall streaks and transport mechanisms (Lee *et al.*, 2013; Patel *et al.*, 2016). Despite these advances, the combined influence of surface roughness and variable thermophysical properties remains largely unexplored, and no unified framework currently exists to describe their coupled effect on momentum and heat transfer.

Here, we present DNS of turbulent channel flow over *Gaussian roughness* using air as the working fluid, including variations in density, viscosity and thermal conductivity. Rough-wall cases are systematically compared with smooth-wall configurations at matched mean-to-wall temperature ratio, enabling a direct assessment of variable-property effects. We analyze the interplay of roughness-induced drag, heat-transfer augmentation, and property-variation effects, with the goal of extending recent transformation frameworks (Modesti & Pirozzoli, 2024) to rough walls and providing a basis for predictive correlations of the friction coefficient and, ultimately, heat transfer.

Case	T_m/T_w	Re_b	Re_τ	$N_x \times N_y \times N_z$	$\Delta x^+ \times \Delta y_w^+ \times \Delta z^+$	k^+	ΔU^+	$\Delta\Theta^+$	$C_f \times 10^2$	$St \times 10^3$
CP-L	1.0	8623	395	$2048 \times 332 \times 1024$	$1.5 \times 0.71 \times 1.5$	64.0	6.36	2.87	1.67	8.10
VP05-L	0.5	26437	411	$2048 \times 332 \times 1024$	$1.6 \times 0.74 \times 1.6$	66.6	5.71	2.12	1.19	5.00
VP07-L	0.7	16133	436	$2048 \times 332 \times 1024$	$1.7 \times 0.79 \times 1.7$	70.6	6.44	2.98	1.45	6.26
VP15-L	1.5	5259	415	$2048 \times 332 \times 1024$	$1.6 \times 0.75 \times 1.6$	67.2	6.96	3.24	1.89	8.80
CP-M	1.0	20008	954	$2048 \times 612 \times 1024$	$3.7 \times 0.67 \times 3.7$	154.6	9.21	3.93	1.81	7.71
VP05-M	0.5	60575	995	$2048 \times 612 \times 1024$	$3.9 \times 0.70 \times 3.9$	161.1	8.01	1.66	1.32	4.44
VP07-M	0.7	38078	1067	$2048 \times 612 \times 1024$	$4.2 \times 0.75 \times 4.2$	172.8	8.91	2.77	1.55	5.47
VP15-M	1.5	13793	1121	$2048 \times 612 \times 1024$	$4.4 \times 0.79 \times 4.4$	181.7	10.45	3.14	2.00	7.47
CP-H	1.0	32295	1563	$2048 \times 908 \times 1024$	$6.1 \times 0.74 \times 6.1$	253.2	10.56	3.58	1.86	7.13
VP05-H	0.5	89334	1515	$2048 \times 908 \times 1024$	$5.9 \times 0.71 \times 5.9$	245.5	9.19	0.59	1.41	4.06
VP07-H	0.7	59145	1671	$2048 \times 908 \times 1024$	$6.5 \times 0.79 \times 6.5$	270.7	9.86	1.80	1.58	4.89
VP15-H	1.5	22127	1784	$2048 \times 908 \times 1024$	$6.8 \times 0.82 \times 6.8$	289.1	11.77	1.63	1.97	6.31

Table 1. Summary of mean-to-wall temperature ratio T_m/T_w, bulk Reynolds number $Re_b = 2\rho_b u_b h/\mu_m$, friction Reynolds number $Re_\tau = \rho_w u_\tau h/\mu_w$, inner-scaled roughness height k^+, roughness functions ΔU^+, $\Delta\Theta^+$, friction coefficient $C_f = 2\tau_w/\rho_b u_b^2$, and Stanton number $St = q_w/\rho_b c p u_b (T_w - Tm)$ for rough channels under constant- (CP) and variable-property (VP) conditions. The suffixes "-L", "-M" and "-H" refer to the low-, medium- and high-Reynolds-number cases, respectively. Roughness functions are computed against their respective variable-property case with smooth walls.

METHODOLOGY

We consider turbulent channel flow of air, modeled as an ideal gas with temperature-dependent viscosity and thermal conductivity at low speeds (bulk Mach number $M_b = 0.2$). The governing equations are the compressible Navier–Stokes equations in conservative form, solved with the high-order solver STREAmS-2.1 (Bernardini *et al.*, 2023; Salvadore *et al.*, 2025). The fluid is a polytropic ideal gas, its Prandtl number is $Pr = 0.72$ and its specific heat ratio is $\gamma = 1.4$. Convective fluxes are discretized with energy-conserving finite differences (Pirozzoli, 2010), while time advancement relies on a low-storage third-order Runge–Kutta scheme.

The computational domain is a plane channel bounded by rough walls. The surface roughness is generated as a three-dimensional Gaussian random field, statistically homogeneous in the streamwise and spanwise directions. The roughness geometry is represented using the *immersed boundary method* (IBM), which enforces no-slip, isothermal conditions at the rough surface while retaining the efficiency of a Cartesian mesh. Mean flow quantities are defined using Favre averaging. Different values of the mean-to-wall temperature ratio are considered in the present simulations, namely $T_m/T_w = 0.5, 0.7$ and 1.5, with T_m being the mixed mean temperature defined as

$$T_m = \frac{1}{2h\rho_b u_b} \int_0^{2h} \overline{\rho}\tilde{u}\widetilde{T}\,\mathrm{d}y, \qquad (1)$$

and ρ_b, u_b are respectively the bulk density and the bulk velocity of the flow.

For each temperature ratio, three friction Reynolds numbers are considered, i.e. $Re_\tau \approx 400, 1000, 1500$. The corresponding results are also compared with constant-property simulations where temperature is modeled as a passive scalar (with $Pr = 0.72$), in order to isolate the role of variable-property effects. The momentum equation is forced to keep a constant mass-flow rate in time. Similarly, the entropy equation is forced to maintain a constant mixed mean temperature. The constant-property simulation is carried out at a friction Reynolds number $Re_\tau \approx 395$ matching the data of Jelly & Busse (2019), approaching the fully rough regime. The statistical properties of the Gaussian rough surface are also chosen to be identical to the reference study (Jelly & Busse, 2019), in order to ensure a consistent comparison. The size of the computational domain used in this study is $L_x \times L_y \times L_z = 8h \times 2h \times 4h$, where L_x, L_y, L_z are the domain extensions in the streamwise, wall-normal and spanwise directions, and h is the channel half-width. The number of grid points was chosen based on a preliminary refinement study, validated against the reference data of Jelly & Busse (2019), which showed very good agreement with the benchmark (not shown for brevity). The number of grid points in each Cartesian direction toghether with the corresponding grid spacings in viscous units is reported in Table 1. The primary observables are the mean streamwise velocity U and temperature profiles $\Theta = T - T_w$, the friction coefficient C_f, the Stanton number St, and the roughness functions ΔU^+ and $\Delta\Theta^+$. Flow statistics are obtained by computing streamwise and spanwise intrinsic averages. The low- and medium-Reynolds-number simulations are averaged over ten eddy-turnover times, defined as $ETT = u_\tau T_s/h$, where T_s is the sampling time window. For the high-Reynolds-number cases, the averaging window corresponds to five eddy-turnover times.

RESULTS

We begin by inspecting the instantaneous streamwise velocity and temperature fields in figure 1, shown in cross-stream and wall-parallel planes for the constant-property case (panels (a,c)) and the variable-property cooled case (panels (b,d)). The presence of roughness elements markedly alters the near-wall organization compared to smooth walls: classical near-wall structures are disrupted, and wakes form in the separated regions downstream of the roughness crests. In the cross-stream planes we note flow bulges spanning two opposite walls, and interacting with the smaller structures close to the wall. We immediately note a strong similarity between streamwise velocity and temperature, with the main difference that the latter

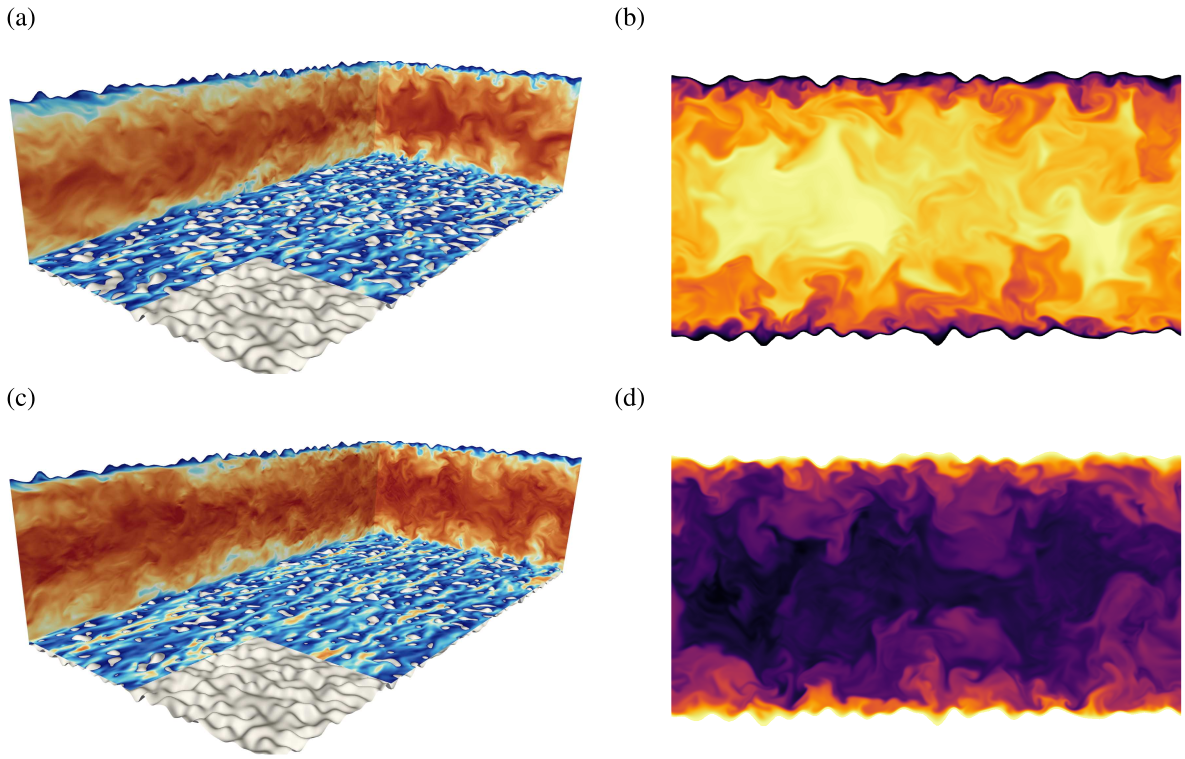

Figure 1. Instantaneous streamwise velocity (a,c) and temperature (b,d) fields for constant-property (a,b) and cooled $T_m/T_w = 0.5$ variable-property (c,d) low-Reynolds cases. Wall-parallel planes are taken 15 wall units from the walls.

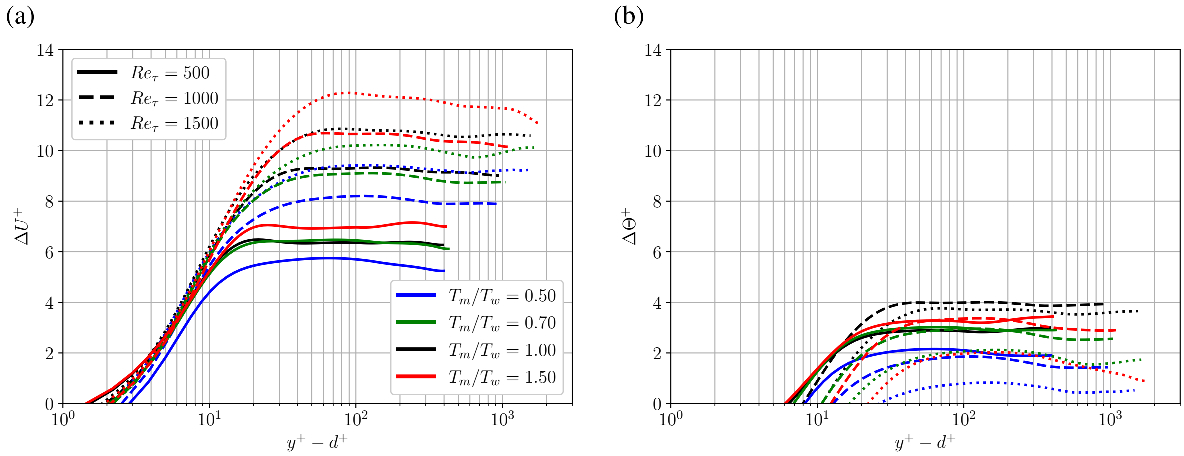

Figure 2. Roughness functions for velocity (a) and temperature (b) fields. Panel (a) shows the Hama function ΔU^+, while panel (b) shows the thermal shift $\Delta\Theta^+$. Results are reported for the constant-property (CP) case and for variable-property (VP) cases with different mean-to-wall temperature ratios T_m/T_w and friction Reynolds numbers. Smooth-wall benchmarks are taken from `https://www.thermoturb.com/` (Modesti & Pirozzoli (2024) in `https://doi.org/10.1017/jfm.2024.1098`).

reveals finer structures due to the absence of the smoothing action of the pressure gradient.

The generalized Hama functions ΔU^+ and $\Delta\Theta^+$ are now assessed. Smooth wall profiles at matched T_m/T_w from the predictive tool `https://www.thermoturb.com/` (based on the work by Modesti & Pirozzoli (2024) in `https://doi.org/10.1017/jfm.2024.1098`) are used to calculate velocity and temperature deficits in figure 2, which are approximately constant in the logarithmic region. The evaluation of ΔU^+ and $\Delta\Theta^+$ includes the virtual-origin (d^+) correction, determined by maximizing the extent of the logarithmic plateau, thus providing a consistent estimate of the roughness functions.

For the constant-property case at the lowest friction Reynolds number we find $\Delta U^+ \simeq 6.4$ and $\Delta\Theta^+ \simeq 2.9$. When variable-property effects are introduced, heating and cooling must be considered separately, as they involve different physical mechanisms. In the cooling regime ($T_m/T_w < 1$), the roughness function ΔU^+ is initially very close to the constant-property case, taking a similar value of approximately 6.4 at $T_m/T_w = 0.7$, and then dropping to 5.7 at $T_m/T_w = 0.5$. In the heating regime ($T_m/T_w > 1$), ΔU^+ instead increases, reaching a value close to 7 at $T_m/T_w = 1.5$, indicating a higher total drag. Similarly, at the lowest Reynolds number, the roughness function $\Delta\Theta^+$ remains close to the constant-property value for $T_m/T_w = 0.7$. For the lowest temperature ratio it decreases, taking values between 3.0 and 2.1 in the cooling regime, whereas in the heating regime it increases up to 3.2.

At higher Reynolds numbers the velocity roughness function retains the same qualitative ordering with the temperature ratio. Cooling cases ($T_m/T_w < 1$) produce systematically smaller values of ΔU^+ than the constant-property case, whereas heating ($T_m/T_w > 1$) increases the roughness function. The magnitude of ΔU^+ increases with friction Reynolds number and k_s^+, reaching values above 11 in the highest-Reynolds-number heating case. The behavior of the thermal roughness function $\Delta\Theta^+$, however, changes significantly with increasing Reynolds number. While at the lowest Reynolds number the ordering resembles that of ΔU^+, at higher Reynolds numbers the constant-property case becomes the largest thermal shift. Cooling cases strongly reduce $\Delta\Theta^+$, which drops to values below 1 at the highest Reynolds number for $T_m/T_w = 0.5$, whereas the heating case remains closer to the constant-property level. This indicates that variable-property effects have a much stronger impact on the thermal roughness function than on the velocity roughness function at high Reynolds numbers.

It is important to stress that ΔU^+ and $\Delta\Theta^+$ are defined with respect to the corresponding variable-property smooth cases. Therefore, drag variations and heat-transfer changes relative to the constant-property case must also be quantified through the friction coefficient C_f and the Stanton number St, as summarized in Table 1.

In variable-property flows, classical wall scaling based on constant density and viscosity is no longer sufficient to collapse the mean velocity and temperature profiles. Variations of density, viscosity and thermal diffusivity modify both viscous transport and turbulent fluxes, leading to systematic departures from the universal law of the wall when profiles are expressed in conventional wall units. Following Modesti & Pirozzoli (2024), these effects can be accounted for by mapping the variable-property flow to an equivalent constant-property flow through suitable convolution transformations. These transformations are derived from the mean momentum and energy balance equations and involve kernel functions that incorporate the local density, viscosity and thermal diffusivity variations. The resulting transformed coordinates recover profiles that closely match the constant-property reference distributions over the entire wall-normal extent of the channel. In the following, we employ these transformations to interpret the velocity and temperature roughness functions obtained in the present simulations.

To account for variable-property effects, the velocity profiles are also reported using the classical van Driest transformation and the HLPP-type transformation (Hasan *et al.*, 2023) introduced by Modesti & Pirozzoli (2024). The van Driest transformation accounts only for density variations and modifies the velocity scaling while leaving the wall-normal coordinate unchanged. The transformed velocity is defined as

$$u_{VD} = \int_0^{\tilde{u}} \sqrt{R}\, \mathrm{d}\tilde{u}, \quad R = \frac{\bar{\rho}}{\bar{\rho}_w}. \tag{2}$$

In contrast, the HLPP transformation accounts for both density and viscosity variations and maps the variable-property flow to an equivalent constant-property flow through convolution integrals applied to the wall-normal coordinate and the Favre-averaged velocity,

$$y_H = \int_0^y f_H\, \mathrm{d}\eta, \qquad u_H = \int_0^{\tilde{u}} g_H\, \mathrm{d}\tilde{u}. \tag{3}$$

The corresponding kernel functions are

$$f_H = \frac{\mathrm{d}}{\mathrm{d}y}\left(\frac{y}{R^{1/2}N}\right),\ g_H = \left(\frac{1+\nu_T/\nu}{1+\nu_{T,cp}/\nu}\right) RN \frac{\mathrm{d}}{\mathrm{d}y}\left(\frac{y}{R^{1/2}N}\right), \tag{4}$$

with

$$N = \frac{\bar{\nu}}{\nu_w}.$$

The turbulent eddy viscosities entering the kernel functions follow the model proposed by Modesti & Pirozzoli (2024).

The resulting velocity roughness functions obtained using the three scalings are reported in Fig. 3. Panel (a) shows the roughness function computed from the untransformed local velocity profiles, panel (b) from the Van Driest transformed profiles, and panel (c) from the HLPP-type transformation of Modesti & Pirozzoli (2024). The error bars indicate the range obtained when the roughness function is evaluated using transformations computed starting from the valley and from the crest of the roughness elements. They therefore represent the variability associated with the choice of the reference roughness height and should not be interpreted as statistical confidence intervals. The equivalent sand-grain roughness height k_s is determined by fitting the constant-property DNS data to the Nikuradse (Nikuradse, 1933) correlation. The resulting value $k_s/k = 1$ indicates that the present roughness reproduces the behavior of the canonical Nikuradse sand-grain roughness.

Overall, the agreement with the incompressible constant-property reference of Nikuradse (1933) is good for all scalings. However, some differences between the transformations can be observed. The HLPP-type transformation provides the closest collapse of the present variable-property data with the incompressible reference behaviour, while the van Driest transformation yields a slightly larger scatter. The roughness function obtained from the untransformed local profiles pheraps shows the largest deviations from the incompressible trend. Interestingly, the heating case with $T_m/T_w = 1.5$ tends to fall systematically below the Nikuradse fit once the velocity profiles are transformed, whereas the remaining temperature ratios remain in close agreement with the incompressible reference curve.

Figure 4 reports the friction coefficient and Stanton number as a function of the bulk Reynolds number. The behavior of the friction coefficient is consistent with the trends observed for the velocity roughness function. In particular, a clear and monotonic ordering with the temperature ratio is preserved across all Reynolds numbers, with heating cases ($T_m/T_w = 1.5$) yielding the highest values of C_f, followed by the constant-property case, and progressively lower values for $T_m/T_w = 0.7$ and 0.5. This behavior reflects the increase or decrease of the effective viscous-scaled roughness height under heating and cooling conditions, which directly impacts the momentum transfer at the wall.

In contrast, the Stanton number exhibits a significantly more complex behavior, with no clear monotonic ordering with respect to the temperature ratio. Although a general decrease of St with increasing Re_b is observed for all cases, the relative position of the different temperature ratios varies with Reynolds number. This reflects the fact that heat transfer is governed by a more intricate balance between molecular diffusion and turbulent transport, which are differently affected by variable-property effects. In particular, cooling tends to reduce the thermal diffusivity and enhance scalar gradients near

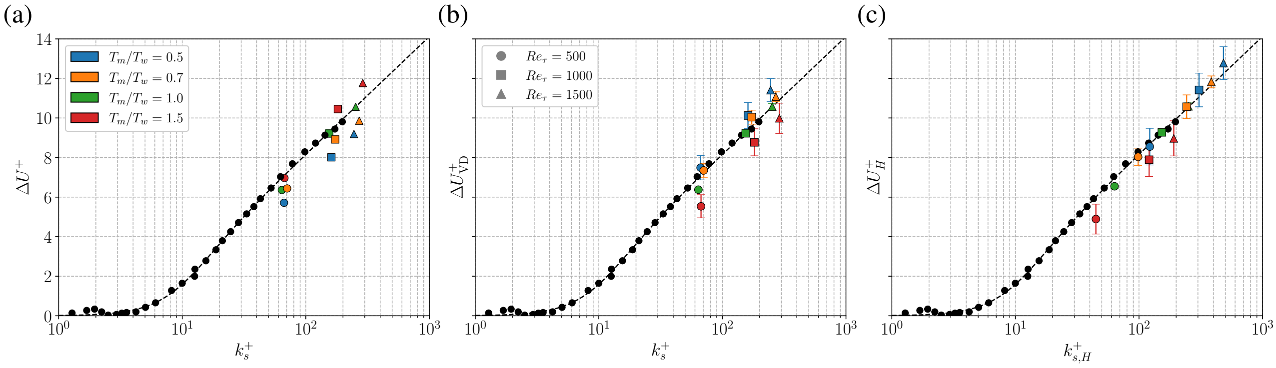

Figure 3. Roughness functions for velocity fields using untransformed local profiles (a), Van Driest transformed profiles (b) and HLPP-like transformed profiles (c). The roughness height is also transformed accordingly in the HLPP-like case. Black symbols and the dashed line denote incompressible reference data from Nikuradse (1933) and the corresponding fit. Error bars indicate the range obtained when the roughness function is evaluated using transformations computed starting from valley to crest. Smooth-wall benchmarks are taken from untransformed and transformed profiles from `https://www.thermoturb.com/` (Modesti & Pirozzoli (2024) in `https://doi.org/10.1017/jfm.2024.1098`).

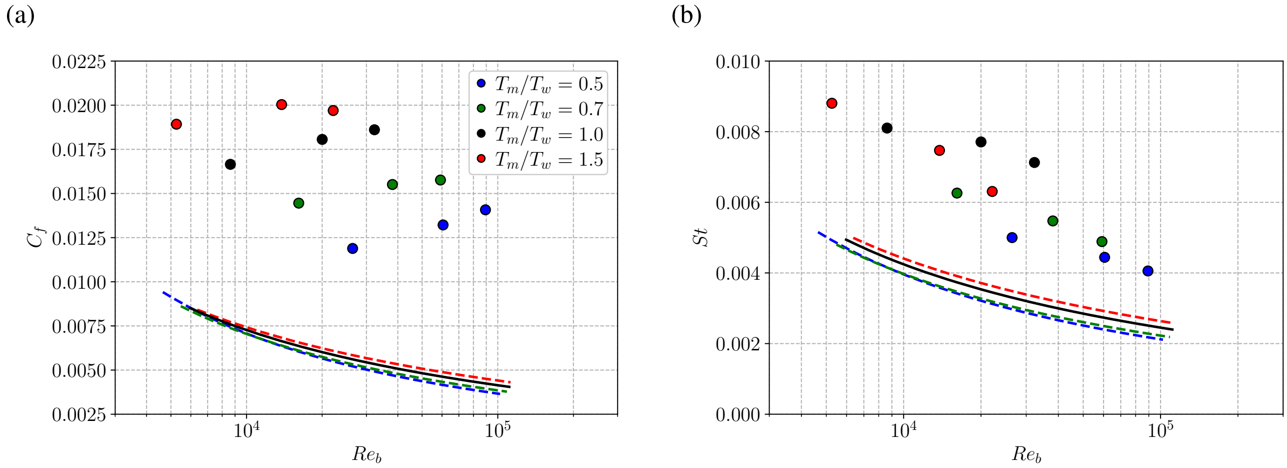

Figure 4. Friction coefficient (a) and Stanton number (b) distributions as function of the bulk Reynolds number for the constant- and variable-properties flow cases. Symboles denote the DNS data while dashed lines denote the smooth trend reference computed from `https://www.thermoturb.com/` (Modesti & Pirozzoli (2024) in `https://doi.org/10.1017/jfm.2024.1098`).

the wall, while heating produces the opposite effect, leading to competing mechanisms that prevent a simple scaling analogous to that observed for momentum transfer. As a result, unlike the friction coefficient, the Stanton number does not follow a universal trend with T_m/T_w, and its behavior cannot be directly inferred from the velocity roughness function alone.

It is also worth noting that the friction coefficient indicates that some of the present cases are approaching the fully rough regime. In contrast, the Stanton number does not exhibit a comparable trend.

CONCLUSIONS & FUTURE WORK

In this work, we have investigated the effect of variable physical properties on turbulent rough-wall channel flows, with particular emphasis on the characterization of the velocity and temperature roughness functions. Direct numerical simulations have been carried out over a range of friction Reynolds numbers and mean-to-wall temperature ratios, allowing a systematic assessment of heating and cooling conditions.

The analysis of the velocity roughness function ΔU^+ shows a remarkable robustness with respect to variable-property effects. In particular, when expressed in terms of the viscous-scaled roughness height, all cases collapse satisfactorily onto the classical incompressible trend, with good agreement with the Nikuradse correlation. This behavior is observed independently of the specific transformation applied to the velocity field, indicating that momentum transfer over rough walls retains a quasi-universal character even in the presence of strong property variations. Variable-property effects primarily manifest as a modulation of the effective viscous scaling, which alters the magnitude of ΔU^+ but does not fundamentally change its dependence on roughness.

In contrast, the thermal roughness function $\Delta\Theta^+$ exhibits a much more complex and non-universal behavior. Its dependence on the temperature ratio and Reynolds number does not follow a clear ordering, highlighting the stronger sensitivity of heat transfer to variable property effects and to the interplay between turbulent transport and molecular diffusion. As a consequence, the direct extension of incompressible correlations to predict $\Delta\Theta^+$ appears to be non-trivial.

Future work will therefore focus on a deeper assessment of the applicability of variable-property velocity transformations, with the aim of establishing a consistent framework for mapping rough-wall flows to an equivalent constant-property reference. In particular, the validity of HLPP-type transformations will be further examined in the presence of surface roughness, including their ability to recover outer-layer similarity. Building on this, a major objective will be the extension of the transformation framework to the thermal field, with the goal of achieving a predictive formulation for $\Delta\Theta^+$ and, ultimately, for the heat transfer coefficient.

To this end, additional simulations will be performed to explicitly assess outer-layer similarity under variable-property conditions. In particular, cases at matched viscous-scaled roughness height k_s^+ but reduced relative roughness k/h (obtained by halving the roughness height in outer units) will be considered. This approach will allow us to disentangle inner- and outer-layer effects and to clarify the role of outer-layer similarity in governing both momentum and heat transfer over rough walls.

REFERENCES

Bernardini, M., Modesti, D., Salvadore, F., Sathyanarayana, S., De Posta, G. & Pirozzoli, S. 2023 Streams-2.0: Supersonic turbulent accelerated navier–stokes solver version 2.0. *Computer Physics Communications* **285**, 108644.

Chung, D., Hutchins, N., Schultz, M. P. & Flack, K. 2021 Predicting the drag of rough surfaces. *Annual Review of Fluid Mechanics* **53**, 439–471.

Dittus, F. & Boelter, L. 1933 Heat transfer in automobile radiators of the tubular type. *International Communications in Heat and Mass Transfer* **12**, 3–22.

Gnielinski, V. 1976 New equations for heat and mass transfer in turbulent pipe and channel flow. *International Chemical Engineering* **16**, 359–367.

Hasan, A., Larsson, J., Pirozzoli, S. & Pecnik, R. 2023 Incorporating intrinsic compressibility effects in velocity transformations for wall-bounded turbulent flows. *Physical Review Fluids* **8** (11), L112601.

Jelly, T. & Busse, A. 2019 Reynolds number dependence of reynolds and dispersive stresses in turbulent channel flow past irregular near-gaussian roughness. *International Journal of Heat and Fluid Flow* **80**, 108485.

Jiménez, J. 2004 Turbulent flows over rough walls. *Annual Review of Fluid Mechanics* **36**, 173–196.

Lee, J., Jung, S., Sung, H. & Zaki, T. 2013 Effect of wall heating on turbulent boundary layers with temperature-dependent viscosity. *Journal of Fluid Mechanics* **726**, 196–225.

Modesti, D. & Pirozzoli, S. 2024 Friction and heat transfer in forced air convection with variable physical properties. *Journal of Fluid Mechanics* **1001**, A27.

Nikuradse, J. 1933 *Stromungsgesetze in rauhen Rohren*, , vol. 361. VDI Forschungsheft.

Patel, A., Boersma, B. & Pecnik, R. 2016 The influence of near-wall density and viscosity gradients on turbulence in channel flows. *Journal of Fluid Mechanics* **809**, 793–820.

Pirozzoli, S. 2010 Generalized conservative approximations of split convective derivative operators. *Journal of Computational Physics* **229** (19), 7180–7190.

Salvadore, F., Soldati, G., Ceci, A., Rossi, G., Memmolo, A., Della Posta, G., Modesti, D., Sathyanarayana, S., Bernardini, M. & Pirozzoli, S. 2025 Streams-2.1: Supersonic turbulent accelerated navier-stokes solver version 2.1. *Computer Physics Communications* **314**, 109652.

Sieder, E. & Tate, G. 1936 Heat transfer and pressure drop of liquids in tubes. *Industrial and Engineering Chemistry* **28** (12), 1429–1435.